scientific reports

OPEN

Multifrequency controlled synchronization of four inductor motors by the fixed frequency ratio method in a vibration system

Lei Jia✉, Chun Wang & Ziliang Liu

In this article, multifrequency controlled synchronization of four inductor motors by the fixed frequency ratio method in a vibration system is investigated. The electromechanical coupling dynamical model of the vibrating system is established. The synchronous condition of the vibrating system is obtained with the small parameter method. Through the theoretical derivation and numerical simulation, multifrequency self-synchronization of four induction motors in the vibration system can't be realized. To achieve the purpose of multifrequency synchronization motion, the method of multifrequency controlled synchronization is proposed, and a fuzzy PID controlling method is introduced. The stability of the controlling system is certified by the Lyapunov criterion. An arbitrariness of the proposed controlling method which is applied to the vibration system is presented. To certify the accuracy of the theory and simulation, a vibrating test bench is constructed. Some experiments are operated to validate the effectiveness and the proposed controlled synchronization method.

With the development of the economy, the pursuit of interest appears to be particularly important in the industry production. For achieving this target, many technologies corresponding to it are presented. In the meanwhile, vibrating machines as a branch in the industry are investigated for benefits on the agriculture, for example, the vibrating screen, the vibrator feeder and so on[1–4]. These kinds of vibrating machines are usually structured by two patterns in the industry. One type as a forced synchronization is realized by belts, gears etc. They can implement the same or different speeds among inductor motors. The other type is based on the self-synchronization theory which is firstly proposed by Blekhman[5,6]. In their research, the dynamic model is combined with the multiscale method which is an asymptotic analytic method based on the average method. By utilizing different time scales, they divide the vibrating motion into two kinds of processes which are respective fast and slow processes. The fast one is relative to the motor speed and the slow one is relative to the phase. Thus, two eccentric rotors (ERs) driven by induction motors realize the self-synchronization on the opposite directions. Obviously, the vibrating machines can be realized with more simple structure and fewer cost by the self-synchronization theory. Based on the former results, many researchers are attracted in this field and it acquires a rapid development. Wen et al.[7] analyses the feature of vibrating system based on a high coupling dynamical model. In addition, they derived synchronous and stability conditions of the vibrating system with the Hamilton criterion. Zhao et al.[8,9] establish the electromechanical coupling dynamic model and converts the problem of synchronous condition into an existence of the eigenvalue with the small parameter average method. They not only realize the self-synchronization motion of two motors in the opposite directions but also in the same directions. The researches above are established in one single rigid body. Zhang et al.[1,10–13] present the theory of self-synchronization with multi motors (more than two motors). In their research, the dynamical model is established based on a rigid body. With the synchronization condition and synchronization criteria of self-synchronization, the characteristic analysis of dynamical model is given. Their research results present that the self-synchronization of vibrating system with three motors can't obtain a superposed amplitude and this phenomenon don't realize the zero differences among three motors. The synchronization problems above are all based on the same frequency of motors. The synchronization problem with different frequency is presented by Inoue Junki chi[14]. In their work, four motors are symmetrically installed on a vibrostand along the vertical axis rather than horizontal axis. And they use this

School of Mechanical Engineering, Shenyang Ligong University, Shenyang 110159, China. ✉email: jialeizsq@126.com

asymmetrical feature to realize the multi-frequency synchronization. However, the mothed in Ref.[14] can only realize one synchronous state with the fixed dynamical model. This result can't satisfy the needs of industry.

The self-synchronization motion which can realize the zero difference between two motors should satisfy the synchronization condition and synchronization criteria. And this result depends on the dynamical feature of the vibrating system. To solve this problem, controlling methods are introduced in the vibrating system. Kong et al.[15,16] introduce the controlling strategy and method into self-synchronization motion and realize the controlled synchronization motion. In their research, a master–slave controlling strategy and an adaptive sliding mode controlling method is presented to be used in the dynamical model of the vibrating system. With this method, the differences of motors which are not zero in the self-synchronization can be realized to zero finally. Besides the method above, Ishizaki et al.[17] use the cross-coupling controlling method to realize the synchronization with dual servo systems. Aiming at the dual linear motor system, Lin et al.[18] apply intelligent complementary sliding mode controlling method to implement cross-coupled synchronous. Attention to different frequency of motors in the synchronization motion, Jia et al.[19,20] propose the adaptive fuzzy PID method and realize the multifrequency controlled synchronization motion. Tian et al.[21] illustrate the fast and robust estimation for positions and velocities by using a generalized modulating functions method. Balthazar et al.[22] gives the research of self-synchronization of four non-ideal exciters. Nanha Djanan et al.[23,24] study the self-synchronization motion on a rectangular plate.

From illustrations above, the purpose of realizing the synchronization motions is to increase the amplitudes of the vibrating system based on the dynamical feature. And this result can be converted to realize the zero differences between motors. However, the multi-frequency synchronization can only be realized with integer frequency (2 or 3 times). For solving this problem, multifrequency controlled synchronization of four inductor motors by fixed frequency ratio method is proposed and the main structure in this article is provided. In section "Mathematical model and synchronization analysis", the dynamical model of the vibrating system with four motors is established. And then synchronization condition and criteria of the vibrating system are both obtained in the least common multiple cycle with the small parameter method. In section "Design of the controlling system", the adaptive fuzzy PID controlling method is introduced in the vibrating system based on a master–slave controlling strategy and the stability of the controlling system is certified by Lyapunov theory. For a legible illustration, some numerical simulations and experiments are shown in section "Numerical and experimental results with discussions" and the conformity between simulation and experiment are listed. In section "Conclusions", some conclusions about this article are given.

Mathematical model and synchronization analysis

Mathematical model of the vibrating system. In this section, the mathematical model of the vibrating system is shown in Fig. 1, which is established from bottom to the top. All the symbols are listed in Table 1. One rigid frame is connected on the foundation with four springs which are symmetrically distributed along coordinate axis. Four squirrel-cage inductor motors divided into two groups are fixed on the frame symmetrically. Motor 1 and 4 as one group have the same frequency and the other group are consisted of motor 2 and 3 of which frequency are different form the front group. Each motor is installed by four bolts through circular holes on the frame.

As shown in Fig. 1, o is center point of the frame and o_i ($i = 1, 2, 3, 4$) are respectively shaft points of four inductor motors. $oo_i = l_i$ ($i = 1, 2, 3, 4$) are respectively the distances between center point of the frame o and shaft points of four inductor motors o_i. m is the quality of the frame and four inductor motors. m_0 is the full quality of each ERs and m_i ($i = 1, 2, 3, 4$) are respectively the actual quality of four ERs. r is the radius of four motors.
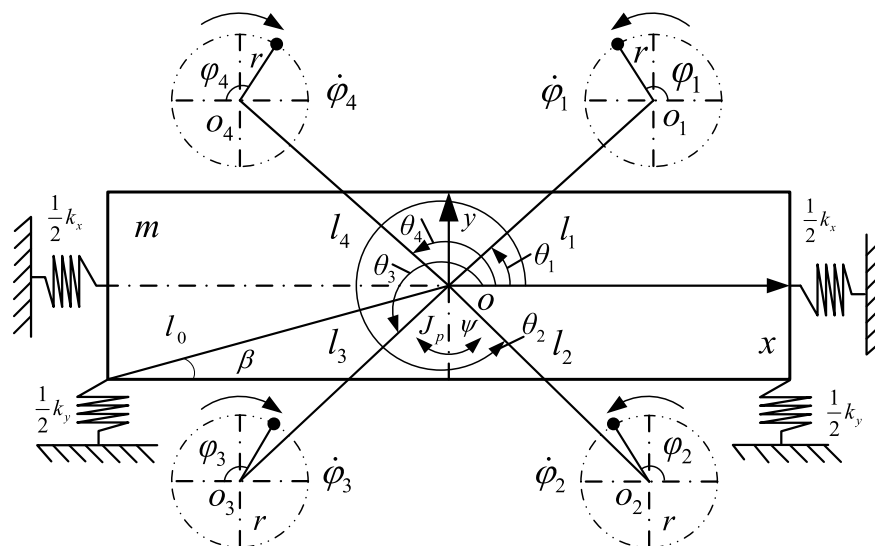

Figure 1. Mathematical model of the vibrating system.

symbol	explanation
m_i	The mass of each ERs
J_p	The moment of inertia of the rigid body
J	The moment of inertia of the vibration system
k_x, k_y, k_ψ	The damping coefficients of the vibration system in the x, y and ψ directions
r	The eccentric radius of the four motors
M	The mass of the total vibration system
f_x, f_y, f_ψ	The stiffness coefficients of the vibration system in the x, y and ψ directions
l_1, l_2, l_3, l_4	The distance between the center of the body and the rotating center of motors
J_i	The moment of inertia of the inductor motor
d-,q-	The d- and q- axes in rotor field-oriented coordinate
L_s	Self-inductance of the stator
L_r	Self-inductance of the rotor
Subscript s	Stator
Subscript r	Rotor
L_m	Mutual inductance of the stator and rotor
ϕ_{sd}	The flux linkages of the stator in the d- axis
ϕ_{sq}	The flux linkages of the stator in the q- axis
ϕ_{rd}	The flux linkages of the rotor in the d- axis
ϕ_{rq}	The flux linkages of the rotor in the q- axis
R_s	The stator resistance
R_r	The rotor resistance
i_{sd}	The current of stator in the d- axis
i_{sq}	The current of stator in the q- axis
i_{rd}	The current of rotor in the d- axis
i_{rq}	The current of rotor in the q- axis
ω	The mechanical speed
ω_s	The synchronous electric angular speed
$\dot{\phi}_{sd}, \dot{\phi}_{sq}, \dot{\phi}_{rd}, \dot{\phi}_{rq}$	Derivation of $\phi_{sd}, \phi_{sq}, \phi_{rd}, \phi_{rq}$
σ	The leakage factor
Tr	A rotor time constant
u_{sd}	The voltage of stator in the d- axis
u_{sq}	The voltage of stator in the q- axis
u_{rd}	The voltage of rotor in the d- axis
u_{rq}	The voltage of rotor in the q- axis
n_p	The number of pole-pairs of the induction motor
$\bullet^*$	The given values or obtained from the given values
$\omega_1, \omega_2, \omega_3, \omega_4$	The speeds of four motors
$\varphi_1, \varphi_2, \varphi_3, \varphi_4$	The phases of four motors
θ	Synchronization electric angle

Table 1. The nomenclature table of the symbols.

$\varphi_i(i = 1, 2, 3, 4)$ are initial phase angle of inductor motors. $\theta_i(i = 1, 2, 3, 4)$ are position angle of four ERs. J_p is rotational inertia of the frame. ψ is the swing angle of the vibrating system. Thus, the differential equation of the vibrating system based on the Lagrange equation can be expressed as

$$\frac{d}{dt}\left(\frac{\partial L}{\partial \dot{\mathbf{q}}}\right) - \frac{\partial L}{\partial \mathbf{q}} = \mathbf{Q} \tag{1}$$

where $L = T - V$. L is the Lagrange function. T and V are respectively the kinetic energy and potential energy. $\mathbf{Q}$ and $\mathbf{q}$ respectively represent generalized force and generalized coordinates. $\mathbf{Q} = (-f_x\dot{x}, -f_y\dot{y}, -f_\psi\dot{\psi}, T_{e1} - f_1\dot{\varphi}_1, T_{e2} - f_2\dot{\varphi}_2, T_{e3} - f_3\dot{\varphi}_3, T_{e4} - f_4\dot{\varphi}_4)^\mathrm{T}$, $\mathbf{q} = (x, y, \psi, \varphi_1, \varphi_2, \varphi_3, \varphi_4)^\mathrm{T}$.

$$T = m(\dot{x} + \dot{y})^2/2 + J_p\dot{\psi}^2/2 + \sum_{i=1}^{4} m_0 \dot{\mathbf{x}}_i^\mathrm{T}\dot{\mathbf{x}}_i/2 + \sum_{i=1}^{4} J_i\dot{\varphi}_i^2/2 \tag{2}$$

In Eq. (2), $\mathbf{x}_i = \begin{pmatrix} x \\ y \end{pmatrix} + \begin{pmatrix} \cos\psi & -\sin\psi \\ \sin\psi & \cos\psi \end{pmatrix}\begin{pmatrix} l_i\cos\theta_i + \tau_i r\cos\varphi_i \\ l_i\sin\theta_i + r\sin\varphi_i \end{pmatrix}$.

3

$$V = k_x x^2/2 + k_y y^2/2 + k_\psi \psi^2/2 \tag{3}$$

Combined Eq. (1) with Eqs. (2) and (3), the electromechanical coupling dynamical model of the vibrating system can be obtained.

$$M\ddot{x} + f_x\dot{x} + k_x x = \sum_{i=1}^{4} \tau_i m_i r(\dot{\varphi}_i^2 \cos\varphi_i + \ddot{\varphi}_i \sin\varphi_i)$$

$$M\ddot{y} + f_y\dot{y} + k_y y = \sum_{i=1}^{4} m_i r(\dot{\varphi}_i^2 \sin\varphi_i - \ddot{\varphi}_i \cos\varphi_i) \qquad , \quad \tau_i = \begin{cases} +1, & i = 1, 2 \\ -1, & i = 3, 4 \end{cases} \tag{4}$$

$$J\ddot{\psi} + f_\psi\dot{\psi} + k_\psi \psi = \sum_{i=1}^{4} m_i r l_i[\dot{\varphi}_i^2 \sin(\varphi_i - \tau_i\theta_i) - \ddot{\varphi}_i \cos(\varphi_i - \tau_i\theta_i)]$$

$$J_i\ddot{\varphi}_i + f_i\dot{\varphi}_i = T_{ei} - T_{Li}$$

where $M = m + \sum_{i=1}^{4} m_i$ is the total mass of the vibrating system, $J = Ml_e^2 \approx J_p + \sum_{i=1}^{4} m_i(l_i^2 + r^2)$ is the equivalent rotational inertia of the vibrating system. l_e is the equivalent rotational radius. $J_i = m_i r^2 (i = 1, 2, 3, 4)$ are respectively rotational inertia of four motors. f_x, f_y and f_ψ are respectively the damping coefficients of vibrating system in x, y and ψ directions, $f_\psi = f_x l_y^2 + f_y l_x^2$. k_x, k_y and k_ψ are respectively the stiffness coefficients of vibrating system in x, y and ψ directions, $f_\psi = f_x l_y^2 + f_y l_x^2$. $f_i(i = 1, 2, 3, 4)$, $T_{ei}(i = 1, 2, 3, 4)$, and $T_{Li}(i = 1, 2, 3, 4)$ are respectively damping coefficients, electromagnetic torques and load torques of four motors. The item T_L in Eq. (4) can be derived as Eq. (5).

$$T_{Li} = m_i r[\ddot{y}\cos\varphi_i - \tau_i\ddot{x}\sin\varphi_i + l_i\ddot{\psi}\cos(\varphi_i - \tau_i\theta_i) + \tau_i l_i\dot{\psi}^2\sin(\varphi_i - \tau_i\theta_i)] \tag{5}$$

Aiming to illustrate the item T_e in the electromechanical coupling dynamical model, the model of inductor motor is given. In this article, the ERs are driven by squirrel-cage inductor motors. With the feature of this kind of inductor motor, its inner rotor windings short-circuit. Thus, $u_{rd} = u_{rq}$. When the motor is at a stable state, ϕ_{rd} = constant and ϕ_{rq} = 0. According to document[25], the model of the inductor motor can be expressed as Eq. (6).

$$L_{ks}di_{sd}/dt = u_{sd} - R_{ks}i_{sd} + R_r L_m/L_r^2\phi_{rd} + \omega_s L_{ks}i_{sq}$$

$$L_{ks}di_{sd}/dt = u_{sq} - R_{ks}i_{sq} - L_m/L_r\phi_{rd}\omega - \omega_s L_{ks}i_{sd}$$

$$d\phi_{rd}/dt = 1/T_r(L_m i_{sd} - \phi_{rd}) \tag{6}$$

$$d\theta/dt = L_m i_{sq}/T_r\phi_{rd} + \omega$$

$$T_e = 3L_m\phi_{rd}i_{sq}/2L_r$$

where, s and r respectively represent stator and rotor. d- and q- represent d- axis and q- axis in the rotating coordinate frame. i, u and R respectively represent current, voltage and resistance. L_s and L_r are respectively represent self-inductance of the stator and rotor. L_m is mutual inductance of the stator and rotor. T_r is rotor time constant, $T_r = L_r/R_r$. L_{ks} is leakage inductance of the stator, $L_{ks} = L_s - L_m^2/L_r$. R_{ks} is equivalent resistance of the stator, $R_{ks} = R_s + L_m^2 R_r/L_r^2$. θ represents the synchronous flux-linkage angle, $\theta = \int (\omega + \omega_s)dt$. ω represents the mechanical angular velocity. ω_s represents the synchronous electrical angular velocity, $\omega_s = L_m i_{sq}/\phi_{rd}T_r$.

To realize the controlled synchronization, the vector control method is introduced in the controlling system. And the rotor flux-oriented control (RFOC) is shown in Fig. 2 to illustrate the controlling system. In Fig. 2, signs with "$*$" are initial values and in Eq. (5), L_m and ϕ_{rd} are given values. i_{sd} can be calculated by formulation $i_{sd} = \phi_{rd}/L_m$. Therefore, the item T_e is related with the feedback values i_{sq}.
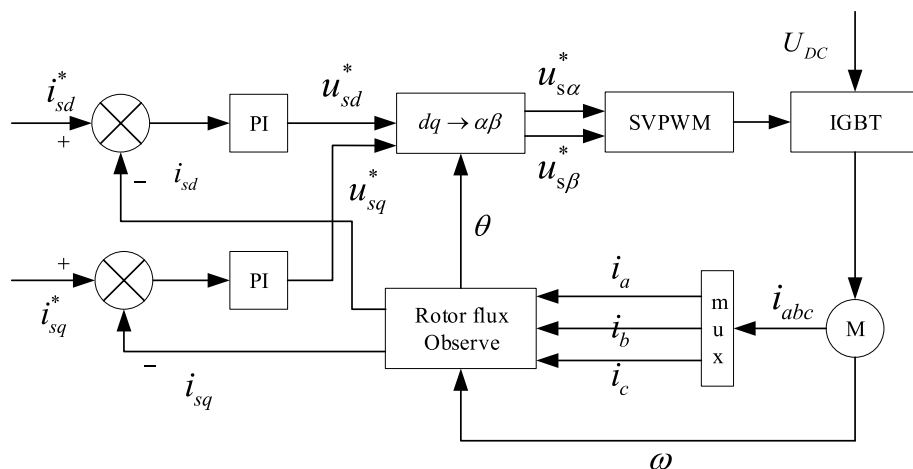

Figure 2. RFOC: rotor flux-oriented control.

Synchronization analysis of the multifrequency self-synchronization. To show the stability analysis of the vibrating system clearly, the illustration of the dynamic model should be given firstly. In this model, motor 1 and motor 4 rotated in the opposite direction as shown in Fig. 1 firstly. When the two motors realize the stable self-synchronization motion with zero phase difference, the stably synchronous state of motor 1 and 4 can be expressed as $\omega_1 - \omega_4 = 0$ and $\varphi_1 - \varphi_4 = 0$. Then Motor 2 and motor 3 finish the same self-synchronization motion as the condition above. In the same way, the stably synchronous state of motor 2 and 3 can be expressed as $\omega_2 - \omega_3 = 0$ and $\varphi_2 - \varphi_3 = 0$. Finally, Motor 1 and 4 realize the multifrequency synchronization motion with the fixed frequency ratio method and the stably synchronous state can be presented as $p\dot{\varphi}_1 - q\dot{\varphi}_2 = 0$ and $n\varphi_1 - \varphi_2 =$ constant. Where, p and q are prime numbers, $p/q = n$. Thus, the speeds of four motors can be presented as

$$\omega_1 = \int_0^{T_1} \dot{\varphi}_1(t)dt/T_1$$
$$\omega_2 = \int_0^{T_2} \dot{\varphi}_2(t)dt/T_2$$
$$\omega_3 = \int_0^{T_3} \dot{\varphi}_3(t)dt/T_3 \tag{7}$$
$$\omega_4 = \int_0^{T_4} \dot{\varphi}_4(t)dt/T_4$$

Taking Eq. (7) into Eq. (4), responses in three directions of the vibrating system can be derived as the Eq. (8).

$$
\begin{aligned}
x = &-r_m r[\eta_1 \cos(\varphi_1 + \gamma_{x1})/\mu_{x1} + \eta_2 \cos(\varphi_2 + \gamma_{x2})/\mu_{x2} - \eta_3 \cos(\varphi_3 + \gamma_{x3})/\mu_{x3} \\
&- \eta_4 \cos(\varphi_4 + \gamma_{x4})/\mu_{x4}] \\
y = &-r_m r[\eta_1 \sin(\varphi_1 + \gamma_{y1})/\mu_{y1} + \eta_2 \sin(\varphi_2 + \gamma_{y2})/\mu_{y2} + \eta_3 \sin(\varphi_3 + \gamma_{y3})/\mu_{y3} \\
&+ \eta_4 \sin(\varphi_4 + \gamma_{y4})/\mu_{y4}] \\
\psi = &-(r_m r/l_e)[\eta_1 r_{l1} \sin(\varphi_1 - \theta_1 + \gamma_{\psi 1})/\mu_{\psi 1} + \eta_2 r_{l2} \sin(\varphi_2 - \theta_2 + \gamma_{\psi 2})/\mu_{\psi 2} \\
&+ \eta_3 r_{l3} \sin(\varphi_3 + \theta_3 + \gamma_{\psi 3})/\mu_{\psi 3} + \eta_4 r_{l4} \sin(\varphi_4 + \theta_4 + \gamma_{\psi 4})/\mu_{\psi 4}]
\end{aligned}
\tag{8}
$$

where $\omega_x^2 = k_x/M$, $\omega_y^2 = k_y/M$, $\omega_\psi^2 = k_\psi/J$, $\zeta_x = f_x/(2\sqrt{k_x M})$, $\zeta_y = f_y/(2\sqrt{k_y M})$, $\zeta_\psi = f_\psi/(2\sqrt{k_\psi J})$, $\mu_{xi} = 1 - \omega_x^2/\omega_i^2$, $\mu_{yi} = 1 - \omega_y^2/\omega_i^2$, $\mu_{\psi i} = 1 - \omega_\psi^2/\omega_i^2$, $r_{li} = l_i/l_e$, $\tan\gamma_{xi} = 2\zeta_x\omega_x/(\mu_{xi}\omega_i)$, $\tan\gamma_{yi} = 2\zeta_y\omega_y/(\mu_{yi}\omega_i)$, $\tan\gamma_{\psi i} = 2\zeta_\psi\omega_\psi/(\mu_{\psi i}\omega_i)$, $r_m = m_0/M$, $\eta_i = m_i/m_0$ $(i = 1, 2, 3, 4)$.

With the small parameter method, the small parameter ε is introduced in Eq. (4). And then, Eq. (4) can be converted to Eq. (9).

$$
\begin{aligned}
J_1\dot{\overline{\varepsilon}}_1\omega_0 + f_1\omega_0(p + \overline{\varepsilon}_1) &= \overline{T}_{e1} - \overline{T}_{L1} \\
J_2\dot{\overline{\varepsilon}}_2\omega_0 + f_2\omega_0(q + \overline{\varepsilon}_2) &= \overline{T}_{e2} - \overline{T}_{L2} \\
J_3\dot{\overline{\varepsilon}}_3\omega_0 + f_3\omega_0(q + \overline{\varepsilon}_3) &= \overline{T}_{e3} - \overline{T}_{L3} \\
J_4\dot{\overline{\varepsilon}}_4\omega_0 + f_4\omega_0(p + \overline{\varepsilon}_4) &= \overline{T}_{e4} - \overline{T}_{L4}
\end{aligned}
\tag{9}
$$

where ω_0 is the average speed of motors in the self-synchronization. The calculation method of $\overline{T}_{ei} = T_{e0i} - k_{e0i}\overline{\varepsilon}_i (i = 1, 2, 3, 4)$ can be obtained from Ref.[15]. Assuming $\dot{\varphi}_1 = (p + \varepsilon_1)\omega_0$, $\dot{\varphi}_2 = (q + \varepsilon_2)\omega_0$, $\dot{\varphi}_3 = (q + \varepsilon_3)\omega_0$, $\dot{\varphi}_4 = (p + \varepsilon_4)\omega_0$, $\ddot{\varphi}_1 = \dot{\varepsilon}_1\omega_0$, $\ddot{\varphi}_2 = \dot{\varepsilon}_2\omega_0$, $\ddot{\varphi}_3 = \dot{\varepsilon}_3\omega_0$, $\ddot{\varphi}_4 = \dot{\varepsilon}_4\omega_0$, the average load torques can be expressed as

$$
\begin{aligned}
\overline{T}_{L1} &= m_0 r^2\omega_0(a_{11}\dot{\overline{\varepsilon}}_1 + a_{14}\dot{\overline{\varepsilon}}_4 + b_{11}\overline{\varepsilon}_1 + b_{14}\overline{\varepsilon}_4 + \kappa_1) \\
\overline{T}_{L2} &= m_0 r^2\omega_0(a_{22}\dot{\overline{\varepsilon}}_2 + a_{23}\dot{\overline{\varepsilon}}_3 + b_{22}\overline{\varepsilon}_2 + b_{23}\overline{\varepsilon}_3 + \kappa_2) \\
\overline{T}_{L3} &= m_0 r^2\omega_0(a_{32}\dot{\overline{\varepsilon}}_2 + a_{33}\dot{\overline{\varepsilon}}_3 + b_{32}\overline{\varepsilon}_2 + b_{33}\overline{\varepsilon}_3 + \kappa_3) \\
\overline{T}_{L4} &= m_0 r^2\omega_0(a_{41}\dot{\overline{\varepsilon}}_1 + a_{44}\dot{\overline{\varepsilon}}_4 + b_{41}\overline{\varepsilon}_1 + b_{44}\overline{\varepsilon}_4 + \kappa_4)
\end{aligned}
\tag{10}
$$

The coefficient and constant items are all listed in the Online Appendix A.

From the Online Appendix A, it can be known that when two inductor motors are with the same frequency (self-synchronization), the coupling effect exists. Otherwise, there is no coupling effect between two motors. Because motor 1 and motor 4 realize self-synchronization motion, the average phase difference can be expressed as $\varphi_1 - \varphi_4 = 2\alpha_1$. Based on the same theory, the average phase difference between motor 2 and motor 3 can be expressed as $\varphi_2 - \varphi_3 = 2\alpha_2$. Take items T_e and T_L into Eq. (10) and expand it at α_1 and α_2 respectively. In the meanwhile, omit the higher order non-liner terms and assume ε_5 and ε_6 to be respectively the small parameter perturbation of two groups of inductor motors. Equation (11) can be obtained.

$$\mathbf{A}\dot{\overline{\boldsymbol{\varepsilon}}} = \mathbf{B}\overline{\boldsymbol{\varepsilon}} + \upsilon \tag{11}$$

where, $\mathbf{A} = \begin{pmatrix} a'_{11} & 0 & 0 & a'_{14} & 0 & 0 \\ 0 & a'_{22} & a'_{23} & 0 & 0 & 0 \\ 0 & a'_{32} & a'_{33} & 0 & 0 & 0 \\ a'_{41} & 0 & 0 & a'_{44} & 0 & 0 \\ 0 & 0 & 0 & 0 & 1 & 0 \\ 0 & 0 & 0 & 0 & 0 & 1 \end{pmatrix}$, $\mathbf{B} = \begin{pmatrix} b'_{11} & 0 & 0 & b'_{14} & b'_{15} & 0 \\ 0 & b'_{22} & b'_{23} & 0 & 0 & b'_{26} \\ 0 & b'_{32} & b'_{33} & 0 & 0 & b'_{36} \\ b'_{41} & 0 & 0 & b'_{44} & b'_{45} & 0 \\ \omega_0/2 & 0 & 0 & -\omega_0/2 & 0 & 0 \\ 0 & \omega_0/2 & -\omega_0/2 & 0 & 0 & 0 \end{pmatrix}$, $\dot{\bar{\varepsilon}} = \begin{pmatrix} \dot{\bar{\varepsilon}}_1 & \dot{\bar{\varepsilon}}_2 & \dot{\bar{\varepsilon}}_3 & \dot{\bar{\varepsilon}}_4 & \dot{\bar{\varepsilon}}_5 & \dot{\bar{\varepsilon}}_6 \end{pmatrix}^{\mathrm{T}}$,

$\bar{\varepsilon} = \begin{pmatrix} \bar{\varepsilon}_1 & \bar{\varepsilon}_2 & \bar{\varepsilon}_3 & \bar{\varepsilon}_4 & \bar{\varepsilon}_5 & \bar{\varepsilon}_6 \end{pmatrix}^{\mathrm{T}}$, $\upsilon = \begin{pmatrix} \upsilon_1 & \upsilon_2 & \upsilon_3 & \upsilon_4 & 0 & 0 \end{pmatrix}^{\mathrm{T}}$. a'_{ij}, b'_{ij} and $\upsilon_i (i = 1, 2, 3, 4)$ are listed in the Online Appendix B.

When the vibrating system reaches the stable synchronous state, the small parameters $\varepsilon = 0$ and $\dot{\varepsilon} = 0$. Thus, the synchronous condition of four ERs can be expressed as Eq. (12).

$$\begin{aligned} T_{e01} &= f_1 p \omega_0 + m_0 r^2 \omega_0 \kappa_1, |T_{e01}| \leq T_{eN1} \\ T_{e02} &= f_2 q \omega_0 + m_0 r^2 \omega_0 \kappa_2, |T_{e02}| \leq T_{eN2} \\ T_{e03} &= f_3 q \omega_0 + m_0 r^2 \omega_0 \kappa_3, |T_{e03}| \leq T_{eN3} \\ T_{e04} &= f_4 p \omega_0 + m_0 r^2 \omega_0 \kappa_4, |T_{e04}| \leq T_{eN4} \end{aligned} \tag{12}$$

where $T_{eNi} (i = 1, 2, 3, 4)$ are respectively the rated electromagnetic torques of four inductor motors. Because of the stable synchronous state, the result of $\upsilon = 0$ can be obtained. Take $\upsilon = 0$ into Eq. (12), and then Eq. (13) can be acquired.

$$\mathbf{A}\dot{\bar{\varepsilon}} = \mathbf{B}\bar{\varepsilon} \tag{13}$$

As shown in Eq. (11), because the matrix A is a non-singular matrix and the determinant $|\mathbf{A}| \neq 0$, the matrix $\mathbf{A}$ is invertible. Then, Eq. (13) can be expressed as Eq. (14).

$$\dot{\bar{\varepsilon}} = \mathbf{D}\bar{\varepsilon} \tag{14}$$

where $\mathbf{D} = \mathbf{A}^{-1}\mathbf{B}$. Because of $|\lambda \mathbf{I} - \mathbf{D}| = 0$, the characteristic equation of the matrix can be represented as

$$\lambda^6 + d_1 \lambda^5 + d_2 \lambda^4 + d_3 \lambda^3 + d_4 \lambda^2 + d_5 \lambda + d_6 = 0 \tag{15}$$

where $d_j (j = 1, 2, 3, 4, 5, 6)$ and λ are respectively coefficients and characteristic values of the characteristic equation.

When the characteristic equation meets the condition of Hurwitz criterion, the synchronous state of the vibrating system is stable. Otherwise, it is unstable.

Design of the controlling system

Design of the electromechanical coupling system. In this section, the controlling system of the vibrating system is shown as Fig. 3. The master–slave controlling strategy is introduced in the controlled structure and the fuzzy PID method is used in the vector controlling method of the inductor motors[26,27]. Motor 1 is considered as the master motor of the system. Motor 2 and 4 are both considered as the slave motors of motor 1. In the meanwhile, motor 3 is considered as the slave motor of motor 2.
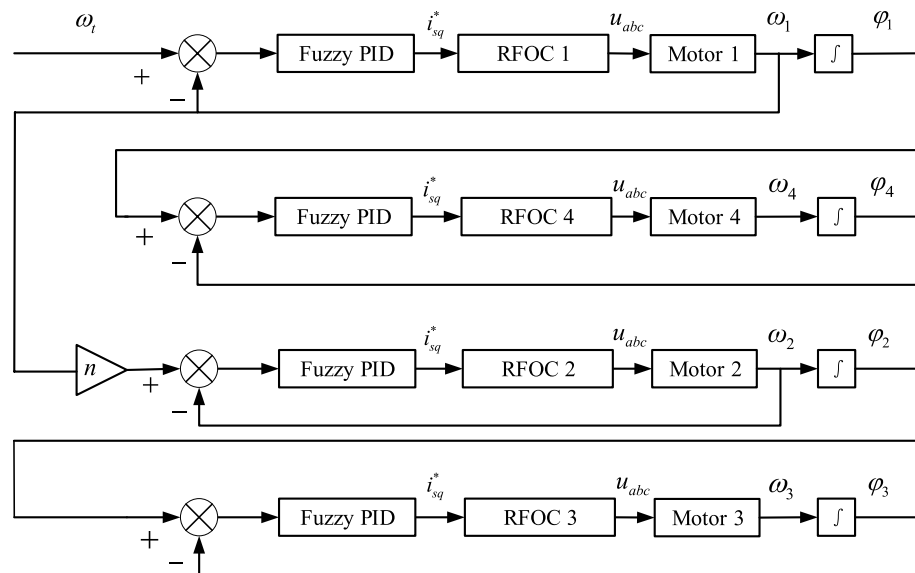

Figure 3. Framework diagram of the controlling system.

To certify the feasibility of the controlling system, Fig. 3 should be illustrated. ω_t as a target speed is given firstly, and then through the fuzzy PID method, the speed of motor 1 ω_1 can be obtained with RFOC 1. There are three functions of ω_1. One is transferred to motor 1 as a feedback value. Another is given to motor 2 as an input value. The other is used to obtain φ_1 through the integral method. With the same frequency, the controlling system is traced through the phase, while it is traced through the speed with the fixed frequency ratio method. Thus, the speeds and phases of motor 2, 3 and 4 can be acquired.

The stability analysis of the controlling system.   Because there are two tracing situations in Fig. 3 which are respectively the speed tracing and phase tracing, the stability of the controlling system should be discussed separately. In the speed tracing situation, the speed of motor is set as the state variable, $\omega = \dot{\varphi}$. Taking $\omega = \dot{\varphi}$ into Eq. (4), thus Eq. (4) can be expressed as

$$J_i \dot{\omega}_i + f\omega_i = K_{Ti} u_i + W_i (i = 1, 2, 3, 4) \tag{16}$$

where $K_{Ti} = L_{mi}\phi_{rdi}/L_{ri}(i = 1, 2, 3, 4)$, u_i as the controlling variable represents i_{qsi}^*, $i = 1, 2, 3, 4$. $W_i = -T_{Li}(i = 1, 2, 3, 4)$ represents the uncertain loads. $J_i(i = 1, 2, 3, 4)$, respectively represents the rotational inertia of four motors. Combined the given target speed ω_t in Fig. 3 with the actual speed ω, the speed error of the motor can be expressed as

$$e = \omega_t - \omega \tag{17}$$

Then, the tracing error of the system can be represented as $\boldsymbol{E} = [e, \dot{e}]^{\mathrm{T}}$. According to Eq. (16), the control law of the system can be designed as

$$u = J/K_T[-\hat{f}(x|\theta_f) + \dot{\omega}_t + \boldsymbol{K}^{\mathrm{T}}\boldsymbol{E} + (f\omega - W)/J] \tag{18}$$

where $\boldsymbol{K} = [k_p, k_i]^{\mathrm{T}}$. The function $\hat{f}(x)$ can be expressed as $\hat{f}(x|\theta_f) = \theta_f^{\mathrm{T}}\xi(x)$ which is based on the weight coefficient θ_f. Thus, the adaptive law of controlling system can be designed as Eq. (19).

$$\dot{\theta}_f = -\gamma \boldsymbol{E}^{\mathrm{T}}\boldsymbol{P}\boldsymbol{b}\xi(\boldsymbol{x}) \tag{19}$$

where $\boldsymbol{P}$ is a positive definite matrix. Considering Ω_f as a convex set to assure the optimal weight coefficient θ_f^* belongs to it and the weight coefficient θ_f is bounded. And then, θ_f^* can be structured as

$$\theta_f^* = \arg \min_{\theta_f \in \Omega_f} [\sup |\hat{f}(x|\theta_f) - f(x)] \tag{20}$$

Taking Eq. (18) into Eq. (16), the closed loop equation of the controlling system is designed as

$$\dot{\boldsymbol{E}} = \boldsymbol{\Lambda}\boldsymbol{E} + \boldsymbol{b}[\hat{f}(x|\theta_f) - f(x)] \tag{21}$$

where $\boldsymbol{b} = \begin{pmatrix} 0 \\ 1 \end{pmatrix}, \boldsymbol{\Lambda} = \begin{pmatrix} 0 & 1 \\ -k_p & -k_i \end{pmatrix}$.

As illuminated in section "Design of the electromechanical coupling system", because the controlling system is a feedback system, the speed error and phase error should be considered. Thus, Eq. (21) can be converted to Eq. (22) which is the approximate error equation with Eqs. (18) and (19).

$$\dot{\boldsymbol{E}} = \boldsymbol{\Lambda}\boldsymbol{E} + \boldsymbol{b}[(\theta_f - \theta_f^*)^{\mathrm{T}}\xi(x) + \Gamma] \tag{22}$$

where $\Gamma = \hat{f}(x|\theta_f^*) - f(x)$ is the minimum approximate error.

To acquire the minimum values of $\boldsymbol{E}$ and $\theta_f - \theta_f^*$, a Lyapunov function is constructed as Eq. (23).

$$V = \boldsymbol{E}^{\mathrm{T}}\boldsymbol{P}\boldsymbol{E}/2 + (\theta_f - \theta_f^*)^{\mathrm{T}}(\theta_f - \theta_f^*)/(2\zeta) \tag{23}$$

where ζ is a positive real number. $\boldsymbol{Q}$ as a positive definite matrix is introduced to satisfy the stability of the Lyapunov equation.

$$\boldsymbol{\Lambda}^{\mathrm{T}}\boldsymbol{P} + \boldsymbol{P}\boldsymbol{A} = -\boldsymbol{Q} \tag{24}$$

Set $V_1 = E^{\mathrm{T}}\boldsymbol{P}E/2$, the derivative $\dot{V}_1 = -E^{\mathrm{T}}\boldsymbol{Q}E/2 + (\theta_f - \theta_f^*)^{\mathrm{T}}E^{\mathrm{T}}\boldsymbol{P}\boldsymbol{b}\xi(x) + E^{\mathrm{T}}\boldsymbol{P}\boldsymbol{b}\Gamma$. Similarly, set $\boldsymbol{V}_2 = (\theta_f - \theta_f^*)^{\mathrm{T}}(\theta_f - \theta_f^*)/(2\zeta)$, and then the derivative $\dot{\boldsymbol{V}}_2 = (\theta_f - \theta_f^*)^{\mathrm{T}}\dot{\theta}_f/\zeta$. Based on the Lyapunov criterion, the derivative of the equation can be expressed as $\dot{\boldsymbol{V}} = \dot{\boldsymbol{V}}_1 + \dot{\boldsymbol{V}}_2$, bring $\boldsymbol{V}_1$ and $\boldsymbol{V}_2$ into $\boldsymbol{V}$, it can be derived as $\dot{V} = -E^{\mathrm{T}}\boldsymbol{Q}E/2 + E^{\mathrm{T}}\boldsymbol{P}\boldsymbol{b}\Gamma$. When the values of Γ which can satisfy the condition $\dot{\boldsymbol{V}} \leq 0$ exist, the system is stable.

With the same method above, the stability certification of speed error and phase error with the other motors can be obtained.

Numerical and experimental results with discussions

In this section, some representative numerical simulation examples are given. The results show that demonstrate that the multifrequency self-synchronization can't be realized. However, the multifrequency controlled synchronization can be realized through the fuzzy PID method. And then, the same results are given with the experiments. The parameters in the simulations and experiments are listed in Tables 2 and 3.

Parameters	Values
M/kg	304
J_p/(kg.m^2)	44.5
k_x/(N/m)	129,332
k_y/(N/m)	105,334
k_ψ/(Nm/rad)	30,715
f_x /(Ns/m)	615.5
f_y/(Ns/m)	618
f_ψ/(Nsm/rad)	180.2
$\theta_1, \theta_2, \theta_3\ \theta_4$ /(°)	30, 150, 210, 330
m_0/kg	6
r/m	0.05
l_1, l_2, l_3, l_4 /m	0.45, 0.45, 0.45, 0.45

Table 2. The parameters in the vibration system.

Parameters	Motor 1	Motor 2	Motor 3	Motor 4
P/kW	0.2	0.2	0.2	0.2
n_p	3	3	3	3
f_0/Hz	50	50	50	50
U/V	220	220	220	220
n/(r/min)	950	950	950	950
R_s/Ω	40.5	40.5	40.5	40.5
R_r/Ω	12	12	12	12
L_s/H	1.21275	1.21275	1.2175	1.21275
L_r/H	1.222	1.222	1.225	1.222
L_m/H	1.116	1.116	1.116	1.116
λ_{dr}^*/Wb	0.98	0.98	0.98	0.98
$f_{1,2,3,4}$/(Nms/rad)	0.005	0.005	0.005	0.005

Table 3. The parameters of four motors.

Results of numerical simulation.   Based on the model of Fig. 1, the frequency of motor 1 and 4 are set as 30 Hz and the frequency of motor 2 and 3 are both 45 Hz. The simulation results in Fig. 4a represent that the speeds of four motors reach the given speeds. From Fig. 4b, it represents that the phase between motor 1 and 4 approximately equals to zero. This result shows that two motors rotated in a opposite direction with the same frequency can reach the stable synchronization state. Similarly, the phase between motor 2 and 3 also trends to zero in Fig. 4c. With the non-linear theory, when the system can achieve $p\dot{\varphi}_1 - q\dot{\varphi}_2 = 0$ and $p\varphi_1 - q\varphi_2 =$ constant, the multifrequency self-synchronization can be realized. However, the phase difference in Fig. 4d is a monotonic curve and $p\varphi_1 - q\varphi_2 \neq$ constant. This result represents that the multifrequency self-synchronization of the vibration system can't be realized. Figure 4e,f are respectively the responses in three directions. The results in Fig. 4 are consistent with the dynamical model.

With the results above, the multifrequency self-synchronization can't be realized. Thus, the fixed frequency ratio method is introduced in the vibrating system. As shown in Fig. 5a is the speeds of four motors. The given speed of motor 1 is 60 rad/s, the speeds of motor 2, 3 and 4 respectively attain 90 rad/s, 90 rad/s and 60 rad/s with the controlling method. Figure 5b is the torque load of four inductor motors. The values of torque loads are between − 2 and 2, so the phenomenon of locked-rotor and overload with motors can't appear. All the inductor motors can operate smoothly. In Fig. 5c, the phase between motor 1 and 4 nearly equals zero, which illustrates motor 1 and 4 reach the stable synchronous state. Figure 5d is phase differences between motor 1 with motor 2 and 3. The phase differences both equal to constants. This result shows that the controlled synchronization is realized with the fixed frequency ratio method. Figure 5e,f are responses in the three directions. In Fig. 5e, two groups of motors both rotate in the opposite direction. Thus, the forces in the y direction counteract with each other and the amplitude in the y direction is nearly to zero, while the amplitudes in the x direction are superimposed. This result accords with the proposed dynamical theory. In Fig. 5f, the response in the ψ direction tends to zero. This phenomenon shows that there is no swing in the vibrating system. Through the Fig. 5, it can be known that the vibrating system reaches the stable synchronous state and the controlled synchronization is realized with the fixed frequency ratio method. To guarantee the arbitrariness of the parameter n, another simulation of which the parameter is altered from 1.5 to 1.2 is presented in Fig. 6. In Fig. 6, the torque loads of four motors still satisfy the operation requirements based on the values between − 1 and 1. Through the speeds and phase differences in Fig. 6a,c,d, the results represent that the vibrating system can realize the controlled
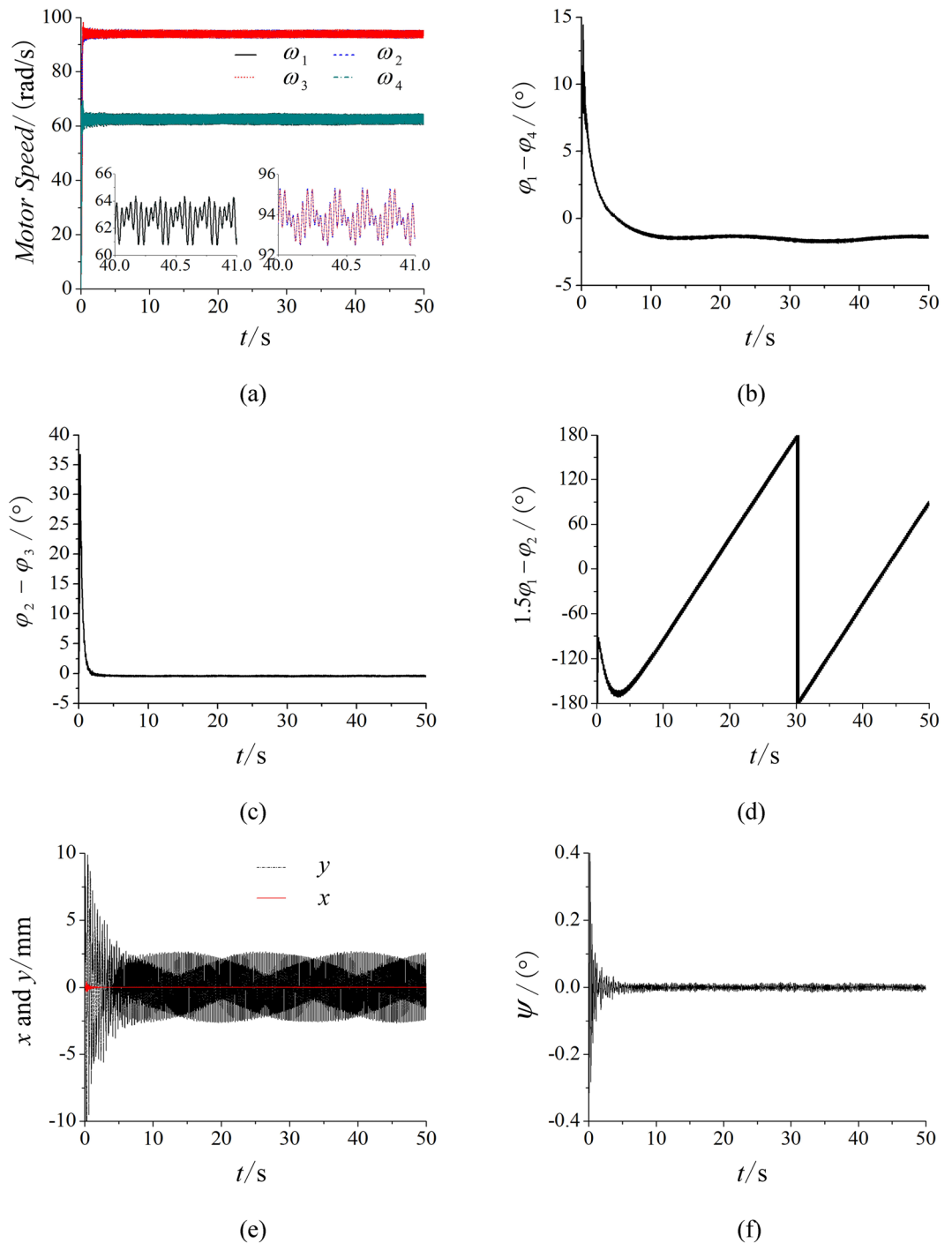
Figure 4. Multifrequency self-synchronization with four ERs, $\alpha_0 = 0$, $n = 1.5$. (**a**) Speed, (**b**) phase difference between motor 1 and 4, (**c**) phase differences between motor 2 and 3, (**d**) phase differences between motor 1 and 2, (**e**) response in the x and y direction, (**f**) response in the ψ direction.

synchronization with the parameter $n = 1,2$. Although the response of the y direction in Fig. 6e is different from the response in Fig. 5 because of the different parameter n, the responses of three directions are still consistent with the dynamical model. So, the vibrating system can realize the stable controlled synchronization. This result demonstrates the arbitrariness of the parameter only if conditions of torque loads are satisfied.

Results of experimental verification. To validate the accuracy of the theory proposed, the main experiment equipment are listed in Fig. 7 firstly. The frequencies of four inductor motors are set by four convertors of
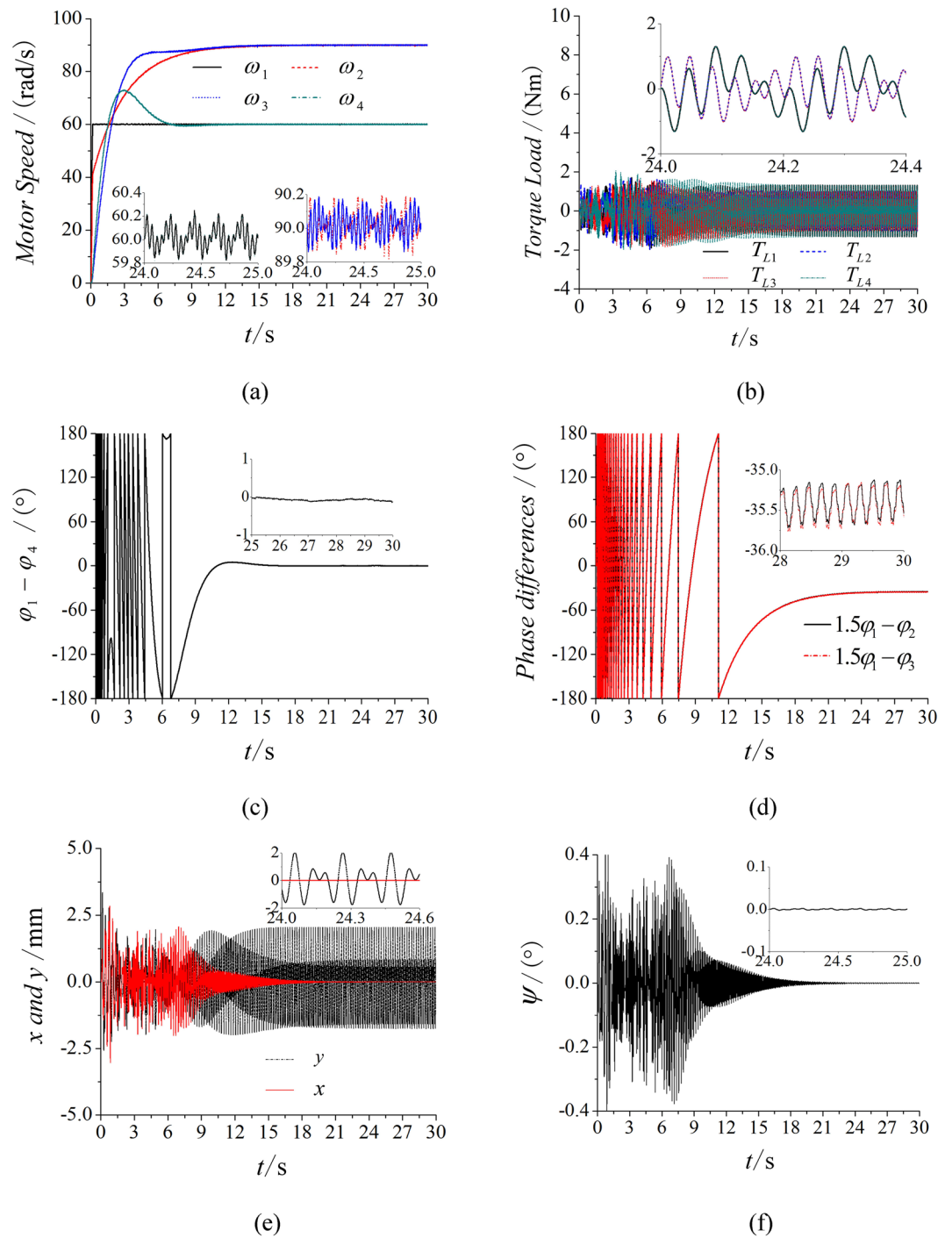
Figure 5. Controlled synchronization with four ERs, $\alpha_0 = 0$, $n = 1.5$, $\eta = 50\%$. (**a**) Speeds, (**b**) load torques, (**c**) phase difference between motor 1 and 4, (**d**) phase differences between motor 1 with motor 2 and 3, (**e**) responses in the x and y direction, (**f**) response in the ψ direction.
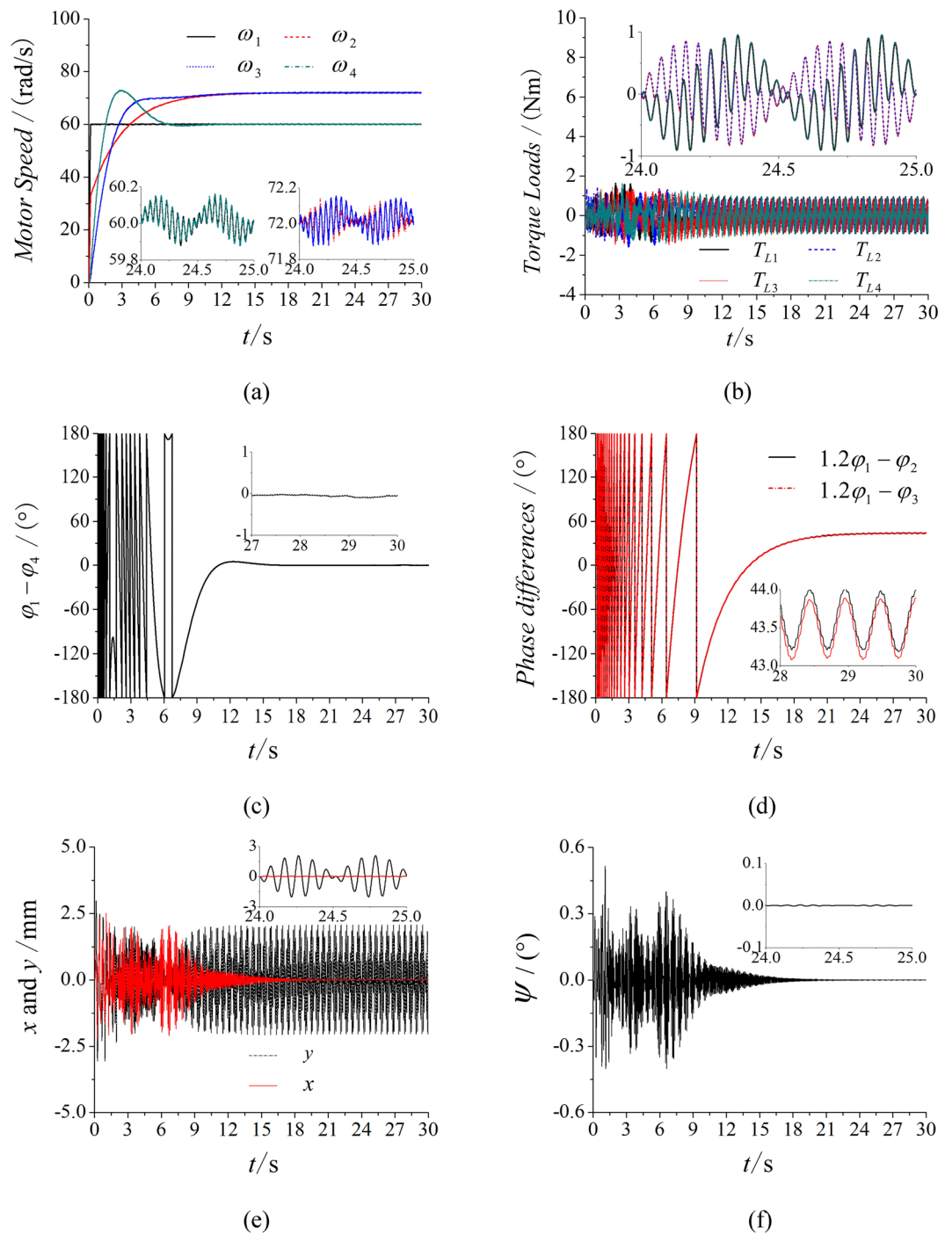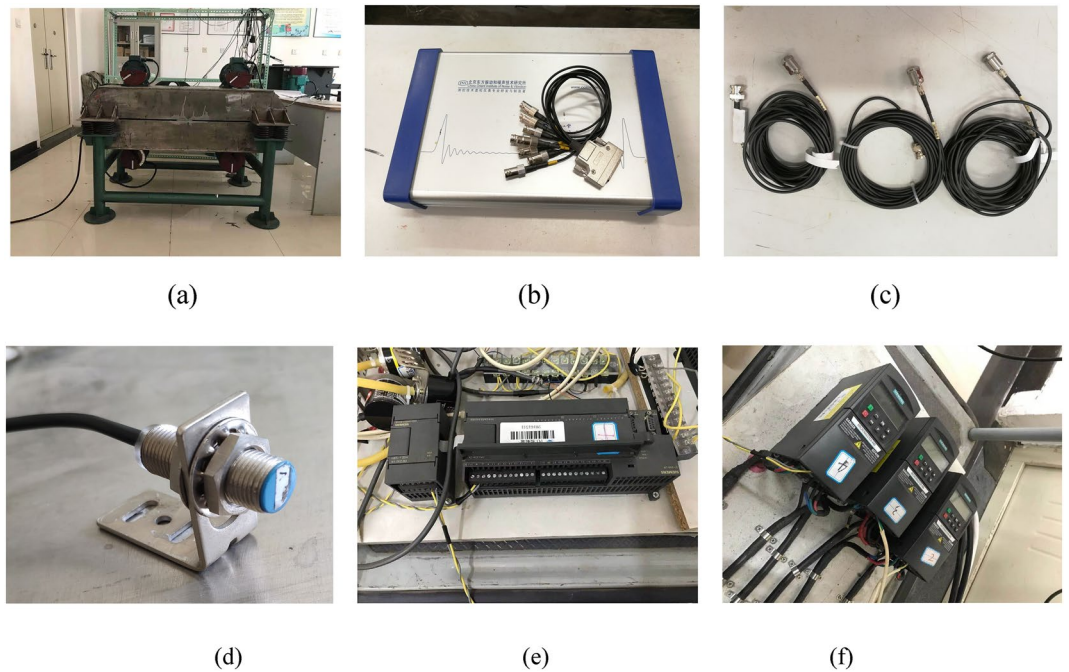
Figure 6. Controlled synchronization with four ERs, $\alpha_0=0$, $n=1.2$, $\eta=50\%$. (**a**) Speeds, (**b**) load torques, (**c**) phase difference between motor 1 and 4, (**d**) phase differences between motor 1 with motor 2 and 3, (**e**) responses in the x and y direction, (**f**) response in the ψ direction.

Figure 7. Experiment equipment of the vibrating system. (**a**) The vibrating testing bench, (**b**) the data acquisition and signal processing, (**c**) the acceleration sensors, (**d**) the Hall magnetic switch, (**e**) the Programmable Logic controller, (**f**) the convertors.

which type are Siemens MM440. The PLC (Programmable Logic controller) are connected with the convertors. The three acceleration sensors are sticked on the vibrating testing bench and connected with the DASP (Data acquisition & signal processing) of which another port is connected with a computer. And then, the experiment of multifrequency self-synchronization is given based on $n = 1.2$ to comparison with the simulation in Fig. 4. As shown in Fig. 8, the frequencies of four motors are respectively set as 30 Hz, 36 Hz, 36 Hz and 30 Hz. From (a), the speeds are stable and reach preset value. Although the difference in (b) is between -5 and -12, motor 1 and 4 can be recognized to realize the self-synchronization motion due to the experiment error. Similar result is in figure (c). Compared with the result in (d) of Fig. 4, (d) in Fig. 8 shows the same result that the curve of the phase difference between motor 1 and 2 is also monotonous. So, the multifrequency self-synchronization can't be realized. The responses of three directions in (e) and (f) are in accordance with the simulation and theory result. This experiment indicates that the multifrequency self-synchronization can't be realized whatever n equals to.

In Fig. 9, the experiment of controlled synchronization is illustrated based on the parameter $n = 1.5$. From Fig. 9a–c, motor 1 with 4 and motor 2 with 3 both realize the controlled synchronization. In Fig. 9d, the phase difference between motor 1 and 2 trends to a constant, which confirms that the controlled synchronization is realized. In Fig. 9e, the response is obviously smaller than the response in Fig. 9g, so this result indicates that the vibrating system realize the stable synchronous state. The response curve of (e) in Fig. 9 is similar with the curve of (e) in Fig. 5 and this experimental result is correspond with the simulation.

Conclusions

The article investigates the multifrequency controlled synchronization of four inductor motors with the fixed frequency ratio method based on a mass-spring rigid body. Through the dynamical model is derived, the stability and synchronization conditions of the vibrating system are both obtained. This result indicates that although the self-synchronization with the same frequency can be realized, the multifrequency self-synchronization of vibrating system can't be realized in the dynamical model of Fig. 1. Some numerical simulations and experiments are given to certify the consistency of the result. Via introducing the proposed the fixed frequency ratio method in the controlling system, the multifrequency controlled synchronization is realized. Through the robustness analysis, the stability of the controlling system is certified to illuminate the feasibility of the controlling method. The conformity of the theory by the simulations and experiments is illustrated. The result indicates that only if the conditions of torque loads can be satisfied, the arbitrariness of the fixed frequency parameter can be realized with the proposed method. Additionally, the multifrequency controlled synchronization method provides a novel way to address the problem of multifrequency vibrating screen in the industry.
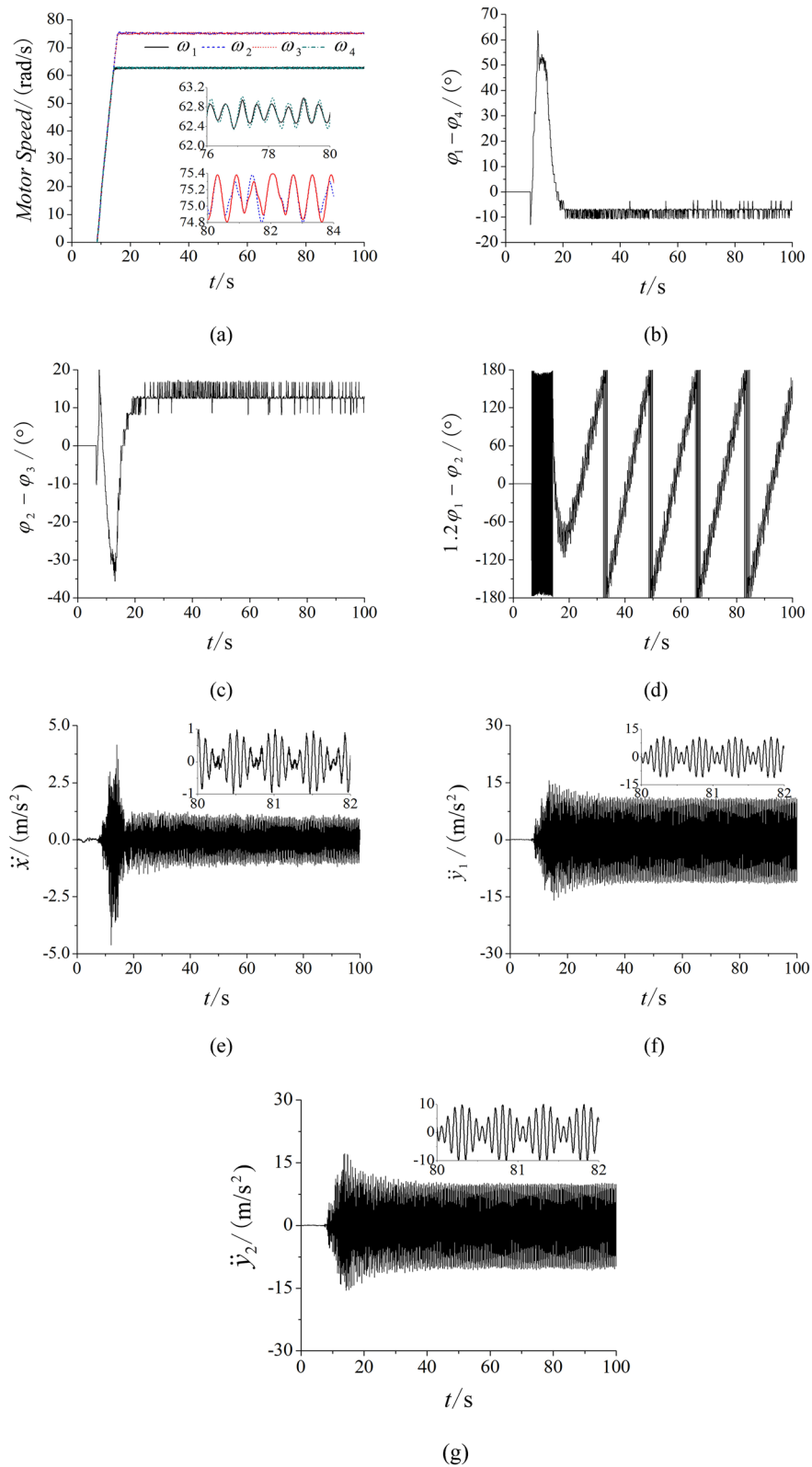
Figure 8. Experiment of multifrequency self-synchronization with four ERs, $\alpha_0=0$, $n=1.2$, $\eta=50\%$. (**a**) Speeds, (**b**) phase difference between motor 1 and 4, (**c**) phase differences between motor 2 and 3, (**d**) phase differences between motor 1 and 2, (**e**) response in the x direction, (**f**) response in the y_1 direction, (**g**) response in the y_2 direction.
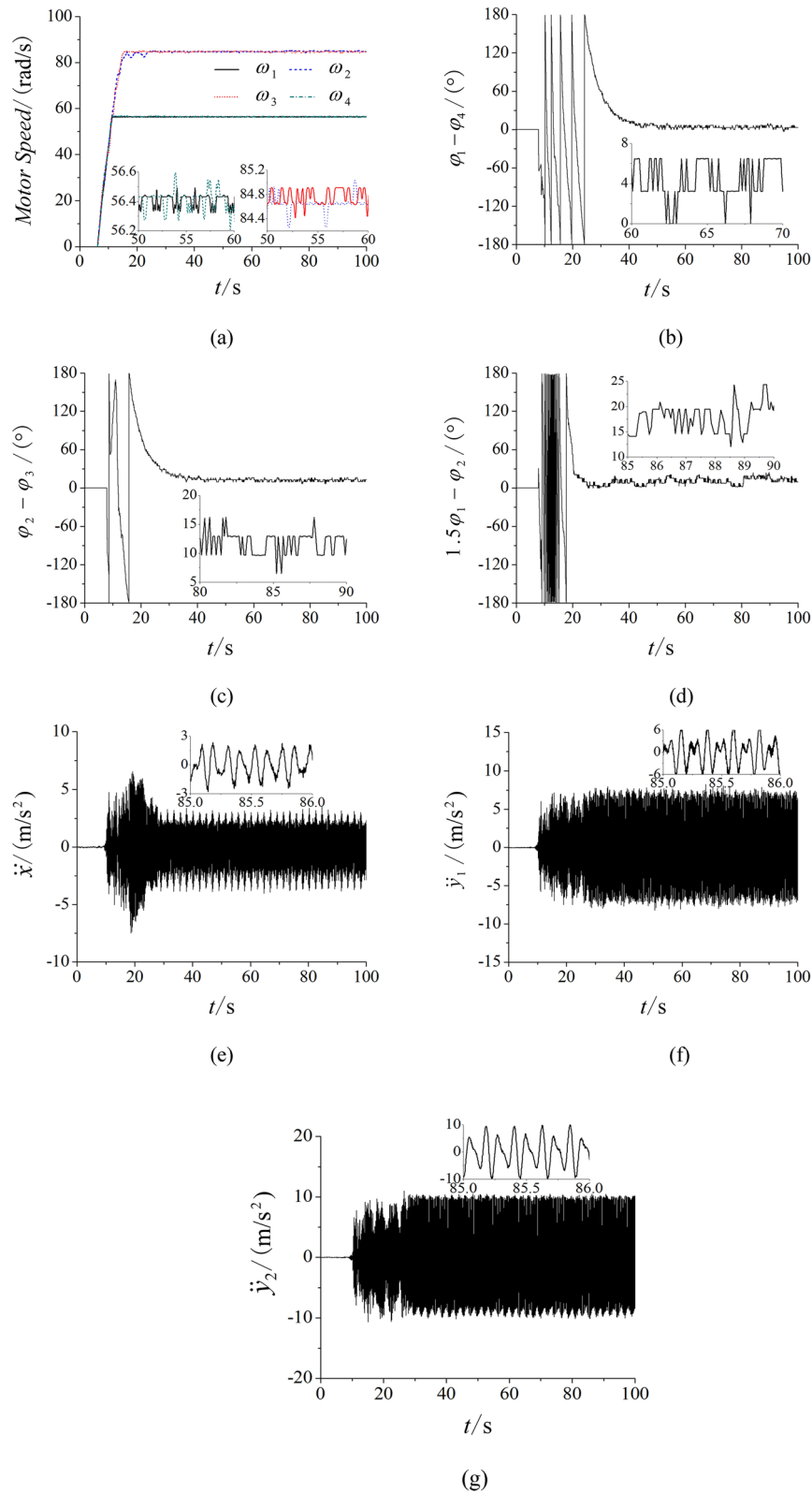
Figure 9. Experiment of controlled synchronization with four ERs, $\alpha_0=0$, $n=1.5$, $\eta=50\%$. (**a**) speeds, (**b**) phase difference between motor 1 and 4, (**c**) phase differences between motor 2 and 3, (**d**) phase differences between motor 1 and 2, (**e**) response in the x direction, (**f**) response in the y_1 direction, (**g**) response in the y_2 direction.

Data availability

The datasets generated during the current study are not publicly available until the project funding in this article is finished, but are available from the corresponding author on reasonable request.

References

1. Zhang, X. L., Wen, B. C. & Zhao, C. Y. Synchronization of three homodromy coupled exciters in a non-resonant vibrating system of plane motion [J]. *Acta. Mech. Sin.* **28**(5), 1424–1435 (2012).
2. Zhao, C. Y., Zhu, H. T., Zhang, Y. M. & Wen, B. C. Synchronization of two coupled exciters in a vibrating system of spatial motion [J]. *Acta. Mech. Sin.* **26**(3), 477–493 (2010).
3. Wen, B. C., Fan, J., Zhao, C. Y. & Xiong, W. L. *Vibratory synchronization and controlled synchronization in engineering [M]* (Science Press, 2009).
4. Kong, X., Zhang, X., Chen, X., Wen, B. & Wang, Bo. Phase and speed synchronization control of four eccentric rotors driven by induction motors in a linear vibratory feeder with unknown time-varying load torques using adaptive sliding mode control algorithm. *J. Sound Vib.* **370**, 23–42 (2016).
5. Blekhman, I. I. Self-synchronization of vibrators in some types of vibrational machines [J]. *Inzhenerny Sbornik* **16**(2), 49–72 (1953) (**in Russian**).
6. Blekhman, I. I. & Sorokin, V. S. On the seperation of fast and show motion in mechanical system with high-frequency modulation of the dissipation coefficient [J]. *J. Sound Vib.* **329**(3), 4936–4949 (2010).
7. Wen, B., Zhang, H., Liu, S., He, Q., & Zhao, C. Theory and techniques of vibrating machinery and their applications (Science Press, 2010).
8. Zhao, C. Y., Zhu, H. T., Wang, R. Z. & Wen, B. C. Synchronization of two non-identical coupled exciters in a non-resonant vibrating system of linear motion Part I: Theoretical analysis[J]. *Shock Vib.* **16**(5), 505–515 (2009).
9. Zhao, C. Y., Zhu, T. T., Bai, T. J. & Wen, B. C. Synchronization of two non-identical coupled exciters in a non-resonant vibrating system of linear motion. Part II: Numeric analysis [J]. *Shock Vib.* **16**(5), 517–528 (2009).
10. Zhang, X. L., Wen, B. C. & Zhao, C. Y. Theoretical, numerical and experimental study on synchronization of three identical exciters in a vibrating system[J]. *Chin. J. Mech. Eng.* **26**(4), 746–757 (2013).
11. Zhang, X. L., Wen, B. C. & Zhao, C. Y. Synchronization of three non-identical coupled exciters with the same rotating directions in a far-resonant vibrating system [J]. *J. Sound Vib.* **332**(9), 2300–2317 (2013).
12. Zhang, X. L., Wen, B. C. & Zhao, C. Y. Experimental investigation on synchronization of three co-rotating non-identical coupled exciters driven by three motors. *J. Sound Vib.* **333**(13), 2898–2908 (2014).
13. Zhang, X. L., Wen, B. C. & Zhao, C. Y. Vibratory synchronization and coupling dynamic characteristics of multiple unbalanced rotors on a mass-spring rigid base[J]. *Int. J. Non-Linear Mech.* **60**, 1–8 (2014).
14. Chi, I. J. On the Self-synchronization of mechanical vibrators: Part 5, Shock vibrator [J]. *J. Japan Soc. Mech. Eng.* **70**(576), 35–42 (1967).
15. Kong, X., Zhang, X., Wen, B. & Wang, Bo. Synchronization analysis and control of three eccentric rotors in a vibration system using adaptive sliding mode control algorithm. *Mech. Syst. Signal Process.* **72–73**, 432–450 (2016).
16. Kong, X., Chen, C. & Wen, B. Composite synchronization of three eccentric rotors driven by induction motors in a vibration system. *Mech. Syst. Signal Process.* **102**, 158–179 (2018).
17. Ishizaki, K., Sencer, B. & Shamoto, E. Cross coupling controller for accurate motion synchronization of dual servo systems [J]. *Int. J. Autom. Technol.* **7**(5), 514–522 (2013).
18. Lin, F. J., Chou, P. H., Chen, C. S. & Lin, Y. S. DSP-based cross-coupled synchronous control for dual linear motors via intelligent complementary sliding mode control [J]. *IEEE Trans. Industr. Electron.* **59**(2), 1061–1073 (2012).
19. Jia, L., Kong, X. X., Zhang, J. Q., Liu, Y. S. & Wen, B. C. Multiple-frequency controlled synchronization of two homodromy eccentric rotors in a vibratory system. *Shock Vib.* **1**, 101–125 (2018).
20. Jia, L., Zhang, J. Q., Zhou, L. H. & Wang, B. C. Multifrequency-controlled synchronization of three eccentric rotors driven by induction motors in the same direction. *J. Low Freq. Noise Vib. Active Control* **38**, 615–632 (2018).
21. Tian, Y., Wei, Y. Q., Liu, D. Y. & Boutat, D. Fast and robust estimation for positions and velocities from noisy accelerations using generalized modulating functions method. *Mech. Syst. Signal Process.* **133**, 106270 (2019).
22. Balthazar, J. M., Palacios Felix, J. L. & Reyolando, M. L. R. F. Some comments on the numerical simulation of self-synchronization of four non-ideal exciters. *Appl. Math. Comput.* **164**, 615–625 (2005).
23. Djanan, A. A. N., Nbendjo, B. R. N. & Woafo, P. Effect of self-synchronization of DC motors on the amplitude of vibration of a rectangular plate. *Eur. Phys. J. Spec. Topics.* **223**, 813–825 (2014).
24. Djanan, A. A. N., Marburg, S. & Nbendjo, B. R. N. On appearance of fast or late self-synchronization between non-ideal sources mounted on a rectangular plate due to time delay. *Math. Comput. Appl.* **27**(2), 20 (2022).
25. Chen, J. *Mathematical model and speed adjustment system of alternating motors* (National Defense Industry Press, 1989).
26. Wang, L.X., & Wang, Y.J. *A course in Fuzzy systems and control* (Prentice hall international editions, 2003).
27. Priyanka, E. B. & Maheswari, C. Online monitoring and control of flow rate in oil pipelines transportation system by using PLC based Fuzzy-PID controller. *Flow Meas. Instrum.* **62**, 144–151 (2018).

Acknowledgements

Author contributions

L.J. finished the dynamical model establishment, experiments and wrote the main manuscript. C.W. prepared all the figures and tables. Z.L. finished the simulations. All authors reviewed the manuscript.

Competing interests

The authors declare no competing interests.

Additional information

Supplementary Information The online version contains supplementary material available at https://doi.org/10.1038/s41598-023-29603-y.

Correspondence and requests for materials should be addressed to L.J.

Reprints and permissions information is available at www.nature.com/reprints.

Publisher's note Springer Nature remains neutral with regard to jurisdictional claims in published maps and institutional affiliations.